Herschel-ATLAS/GAMA: spatial clustering of low-redshift submm galaxies[★]

E. van Kampen,[1]† D. J. B. Smith,[2,3] S. Maddox,[2,4] A. M. Hopkins,[5] I. Valtchanov,[6] J. A. Peacock,[7] M. J. Michałowski,[7] P. Norberg,[8] S. Eales,[9] L. Dunne,[2,4] J. Liske,[1] M. Baes,[10] D. Scott,[11] E. Rigby,[2,7] A. Robotham,[12] P. van der Werf,[7,13] E. Ibar,[14] M. J. Jarvis,[3] J. Loveday,[15] R. Auld,[7] I. K. Baldry,[16] S. Bamford,[2] E. Cameron,[17] S. Croom,[18] S. Buttiglione,[19] A. Cava,[20] A. Cooray,[21] S. Driver,[12,22] J. S. Dunlop,[7] A. Dariush,[23] J. Fritz,[10] R. J. Ivison,[14] E. Pascale,[9] M. Pohlen,[9] G. Rodighiero,[24] P. Temi,[25] D. G. Bonfield,[3] D. Hill,[3] D. H. Jones,[5] L. Kelvin,[12] H. Parkinson,[7] M. Prescott,[16] R. Sharp,[5] G. de Zotti,[19,26] S. Serjeant,[27] C. C. Popescu[28] and R. J. Tuffs[29]

[1]*European Southern Observatory, Karl-Schwarzschild-Strasse 2, D-85748 Garching bei München, Germany*
[2]*School of Physics and Astronomy, University of Nottingham, University Park, Nottingham, NG7 2RD*
[3]*Centre for Astrophysics Research, Science and Technology Research Institute, University of Hertfordshire, Herts AL10 9AB*
[4]*Department of Physics and Astronomy, University of Canterbury, Private Bag 4800, Christchurch, New Zealand*
[5]*Australian Astronomical Observatory, PO Box 296, Epping, NSW 1710, Australia*
[6]*Herschel Science Centre, ESAC, ESA, PO Box 78, Villanueva de la Cañada, 28691 Madrid, Spain*
[7]*SUPA, Institute for Astronomy, University of Edinburgh, Royal Observatory, Blackford Hill, Edinburgh EH9 3HJ*
[8]*Institute for Computational Cosmology, Department of Physics, Durham University, South Road, Durham DH1 3LE*
[9]*School of Physics and Astronomy, Cardiff University, The Parade, CF24 3AA*
[10]*Sterrenkundig Observatorium, Universiteit Gent, Krijgslaan 281 S9, B-9000 Gent, Belgium*
[11]*Department of Physics and Astronomy, 6224 Agricultural Road, University of British Columbia, Vancouver, BC, V6T 1Z1, Canada*
[12]*SUPA, School of Physics and Astronomy, University of St. Andrews, North Haugh, St. Andrews KY16 9SS*
[13]*Leiden Observatory, Leiden University, PO Box 9513, NL-2300 RA Leiden, the Netherlands*
[14]*UK Astronomy Technology Center, Royal Observatory Edinburgh, Edinburgh EH9 3HJ*
[15]*Astronomy Centre, Department of Physics and Astronomy, University of Sussex, Falmer, Brighton BN1 9QH*
[16]*Astrophysics Research Institute, Liverpool John Moores University, 12 Quays House, Egerton Wharf, Birkenhead CH41 1LD*
[17]*ETH Zurich, Insitute for Astronomy, HIT J12.3, CH-8093 Zurich, Switzerland*
[18]*Sydney Institute for Astronomy, School of Physics, University of Sydney, NSW 2006, Australia*
[19]*INAF-Osservatorio Astronomico di Padova, Vicolo Osservatorio 5, I-35122 Padova, Italy*
[20]*Departamento de Astrofísica, Facultad de CC. Físicas, Universidad Complutense de Madrid, E-28040 Madrid, Spain*
[21]*Department of Physics & Astronomy, University of California, Irvine, CA 92697, USA*
[22]*International Centre for Radio Astronomy Research (ICRAR), University of Western Australia, WA 6009, Australia*
[23]*Physics Department, Imperial College London, South Kensington campus, London SW7 2AZ*
[24]*University of Padova, Vicolo Osservatorio 3, I-35122 Padova, Italy*
[25]*Astrophysics Branch, NASA Ames Research Center, Mail Stop 245-6, Moffett Field, CA 94035, USA*
[26]*SISSA, Via Bonomea 265, I-34136 Trieste, Italy*
[27]*Department of Physics and Astronomy, The Open University, Milton Keynes MK7 6AA*
[28]*Jeremiah Horrocks Institute, University of Central Lancashire, Preston PR1 2HE*
[29]*Max Planck Institute for Nuclear Astrophysics (MPIK), Saupfercheckweg 1, 69117 Heidelberg, Germany*

ABSTRACT

We have measured the clustering properties of low-redshift ($z < 0.3$) submm galaxies detected at 250 μm in the *Herschel*-ATLAS science demonstration phase field. We selected a sample

[★] *Herschel* is an ESA space observatory with science instruments provided by European-led Principal Investigator consortia and with important participation from NASA.
†E-mail: evkampen@eso.org

for which we have high-quality spectroscopic redshifts, obtained from reliably matching the 250-μm sources to a complete (for $r < 19.4$) sample of galaxies from the GAMA data base. Both the angular and spatial clustering strength are measured for all $z < 0.3$ sources as well as for five redshift slices with thickness $\Delta z = 0.05$ in the range $0.05 < z < 0.3$. Our measured spatial clustering length r_0 is comparable to that of optically selected, moderately star-forming (blue) galaxies: we find values around 5 Mpc. One of the redshift bins contains an interesting structure, at $z = 0.164$.

Key words: surveys – galaxies: statistics – large-scale structure of Universe – submillimetre: galaxies.

1 INTRODUCTION

A key statistical property of a given population of galaxies is its clustering length, most often expressed as the scale-length of the galaxy–galaxy autocorrelation function. This statistic quantifies the environment of such a galaxy population, and thus helps to interpret their other properties. This paper deals with clustering of low-redshift submm detected galaxies, which are expected to be relatively normal galaxies, albeit with somewhat enhanced star formation as compared to high-redshift submm galaxies, which typically have much higher star formation rates and are thought to be mostly merger-induced star-bursting galaxies.

'Normal', local galaxies, as detected in the optical wavebands, have clustering lengths of 5–6 Mpc, depending on colour and/or luminosity (e.g. Coil et al. 2008 for the DEEP2 sample, Zehavi et al. 2011 for the SDSS DR7 sample and Christodoulou et al. 2012 for an analysis of the SDSS DR7 sample using photometric redshifts calibrated using GAMA data). In this paper we study the clustering properties of galaxies selected at 250 μm for which we also have a spectroscopic redshift (of sufficient accuracy).

For submm galaxies, various clustering estimates exist, most often for samples where redshift information is sparse and only small fields are covered. Early attempts to measure the angular correlation function for high-z submm galaxies detected with Submillimetre Common-User Bolometer Array (SCUBA) include Almaini et al. (2003), Webb et al. (2003), Blain et al. (2004) and Scott, Dunlop & Serjeant (2006). A more recent estimate is that of Weiß et al. (2009), using LABOCA. In this paper we make use of the science demonstration phase (SDP) data of *Herschel*-ATLAS (Eales et al. 2010), which offers a wider area than was available to the studies mentioned above, although at a shorter wavelength (and thus a lower peak redshift). The angular clustering of all reliably detected 250-μm sources in this SDP field has been measured by Maddox et al. (2010). A similar measurement for a similar sample, obtained as part of the HerMES project, was presented by Cooray et al. (2010). Both these measurements have been compared to model predictions by Short & Coles (2011).

Here we study a subset of the galaxies used for the clustering analysis of Maddox et al. (2010): those with reliable spectroscopic redshifts. This allows us to study spatial clustering, although only for redshifts below about 0.3, where we have sufficient numbers of redshifts. In a related, complementary paper, Guo et al. (2011) measure the cross-correlation of a similar sample of galaxies, to study the clustering bias of this sample and the properties of their haloes.

In Section 2 we first describe our particular sample of low-redshift submm sources and how it was selected. In Section 3 we describe the methods to estimate angular and spatial clustering measures, which are then applied in Section 4 to study the clustering properties

of our sample. In Section 5 we summarize our conclusions and look forward to what we can do once the full *Herschel*-ATLAS data set becomes available. In this paper we adopt the following cosmological parameters where needed: $H_0 = 73 \, \mathrm{km \, s^{-1} \, Mpc^{-1}}$, $\Omega_\mathrm{m} = 0.25$ and $\Omega_\Lambda = 0.75$.

2 OBSERVATIONAL DATA

The observational data used come from a match of source catalogues obtained from *Herschel*-ATLAS (Eales et al. 2010) and GAMA (Driver et al. 2011), performed by Smith et al. (2011). In this section we describe the source catalogues and selection.

2.1 *Herschel*-ATLAS data and SPIRE source catalogue

Our sample of low-redshift submm sources is extracted from the first *Herschel*-ATLAS data field that was taken as part of the SDP, as described in Eales et al. (2010). *Herschel*-ATLAS is based on parallel scan mode observations performed with *Herschel* (Pilbratt et al. 2010). Maps from the SPIRE (Griffin et al. 2010) data were produced using a naive mapping technique after removing instrumental temperature variations from the time-line data (Pascale et al. 2011). Noise maps were generated by using the two cross-scan measurements to estimate the noise per detector pass, and then for each pixel the noise is scaled by the square root of the number of detector passes.

Submm sources were identified in the SPIRE maps as described in Rigby et al. (2011). To produce a catalogue of reliable sources, only those that are detected at the 5σ level at 250 μm were selected. In calculating the σ value for each source, the relevant noise map was used, and the confusion noise was added to this in quadrature. The average 1σ instrumental noise values are 4, 4 and 5.7 mJy beam^{-1} respectively in the 250, 350 and 500 μm bands. The confusion noise was estimated from the difference between the variance of the maps and the expected variance due to instrumental noise: the 1σ confusion noise was found to be 5, 6 and 7 mJy beam^{-1} at 250, 350 and 500 μm, in agreement with Nguyen et al. (2010). The resulting total 5σ limits are 33, 36 and 45 mJy beam^{-1}, respectively.

2.2 Redshifts and source selection

Spectroscopic redshifts are taken from the GAMA data base (Driver et al. 2009; Baldry et al. 2010; Robothan et al. 2010; Driver et al. 2011; Hill et al. 2011), which covers most of the *Herschel*-ATLAS SDP field, except for a fraction below declination $\delta = -1°$. These redshifts come from a variety of sources, although most were taken by the GAMA team using 2dF+AAOmega at the Anglo-Australian Telescope (AAT; Driver et al. 2009).

The overlapping area contains 5370 sources for which the SPIRE 250 μm flux is above 5σ (corresponding to 33 mJy). In order to assign spectroscopic redshifts from GAMA, which has the SDSS sample as an input catalogue, to as many of these sources as possible, Smith et al. (2011) matched the SPIRE sources to the SDSS DR7 sample (Abazajian et al. 2009), using a likelihood-ratio analysis (Sutherland & Saunders 1992). All $r < 22.4$ SDSS sources within a 10-arcsec radius of each SPIRE source were considered, taking into account that the true counterpart could be below the optical magnitude limit. In this process, Smith et al. (2011) also calculated a reliability R for any given source to be the correct counterpart, and we follow their recommendation to only use sources with $R \geq 0.8$.

Besides cutting at reliability R, we also select GAMA sources with redshifts of sufficient quality ($Q \geq 3$, see Driver et al. 2011 for a detailed definition of the redshift quality parameter Q), and with $r_{Pet} < 19.4$, which is the Petrosian magnitude cut for which GAMA was designed to be complete in redshift coverage; GAMA has almost achieved that (98.7 per cent completeness for this cut).

We have tried supplementing these redshifts with (available) photometric redshifts from Smith et al. (2011), selecting only those that have uncertainties $\Delta z < 0.05$, which is equal to the size of the redshift bins we chose for our redshift slices (see Section 4.1.2). These redshifts are mostly in the range $0.3 < z < 0.4$, but we found that their number is too few to give a reliable clustering estimate in this range. Also, the additional complexity of taking into account the relatively large redshift errors results in clustering detections that are marginal at best. We therefore chose not to use photometric redshifts for this study.

Summarizing, we selected low-redshift submm galaxies which

(i) are above 5σ at 250 μm (a flux cut of 33 mJy);
(ii) are in the GAMA 9h field;
(iii) have source ID reliability $R \geq 0.8$;
(iv) have spectroscopic redshift quality $Q \geq 3$;
(v) have $r_{Pet} < 19.4$ and
(vi) have $z < 0.3$.

The sample thus constructed, with flux limits in both optical and submm bands, leads to a somewhat specialized selection. In particular at the faint end we select galaxies that are either red, dusty or both. For our spectroscopic redshifts we are restricted to $r_{Pet} < 19.4$ galaxies, but we do have photometric redshifts for many galaxies beyond that (Smith et al. 2011). This allows us to estimate the minimum fraction of low-redshift submm galaxies missed in our analysis (i.e. those with $r_{Pet} > 19.4$ but with a low photometric redshift) for each of the redshift slices considered. For the *Herschel*-ATLAS Phase 1 data set, which is much larger than the SDP data set considered here, photometric redshifts have recently been estimated (Pearson et al. 2012) for galaxies down to $r_{Pet} \approx 20.8$, giving sufficient depth and width to give a reasonable incompleteness estimate for our low-redshift submm samples, even though this is a lower limit (there will still be low-redshift submm galaxies with $r_{Pet} > 20.8$, although we do not expect this fraction to be large).

Performing this analysis for the G09 Phase 1 field, we find a minimum incompleteness fraction of 14 per cent for $z < 0.3$, where this fraction is very low at the lowest redshift end, and around 40 per cent near $z = 0.3$. These and additional fractions are given and discussed in the relevant sections below.

The top panel of Fig. 1 shows all 5σ SPIRE sources within the GAMA field (using just the first two criteria that are listed above), most of which are not actually identified in the GAMA source
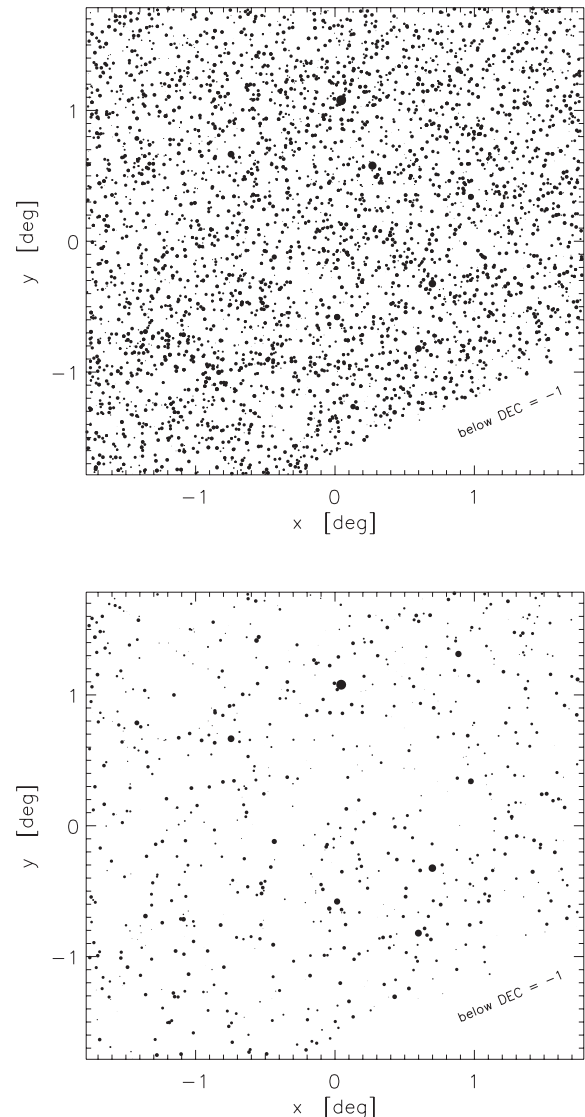

Figure 1. Top panel: sky distribution of all 250-μm sources above 33 mJy that overlap with the GAMA field. These sources cover a wide range of redshifts. Bottom panel: those sources with spectroscopic redshifts of sufficient quality (see the main text for details), $r_{Pet} < 19.4$ and $z < 0.3$. Both panels were rotated by 25° to take into account the orientation of the *Herschel* SDP field, and have no sources in the bottom-right corner which is not covered by GAMA. Symbol sizes are (inversely) proportional to the submm magnitude at 250 μm.

catalogue. 5σ SPIRE sources that are identified as GAMA sources, have $r_{Pet} < 19.4$, $z < 0.3$, and are sufficiently reliable matches with good quality redshifts ($R \geq 0.8$ and $Q \geq 3$), are shown in the bottom panel of Fig. 1. Both panels were rotated by 25° to take into account the orientation of the *Herschel* SDP field. The corner region below $\delta = -1°$ is the area that is not part of the GAMA survey, and therefore disregarded for the purpose of this paper.

The redshift distribution of the sources with GAMA redshifts is shown in Fig. 2 (all criteria except the last have been applied). Beyond $z = 0.3$ the number of spectroscopic redshifts (thin histogram in Fig. 2) quickly decreases, so we restrict ourselves to $z < 0.3$ in this paper.

For the purpose of estimating the spatial clustering length through the Limber equation inversion method (which involves numerical
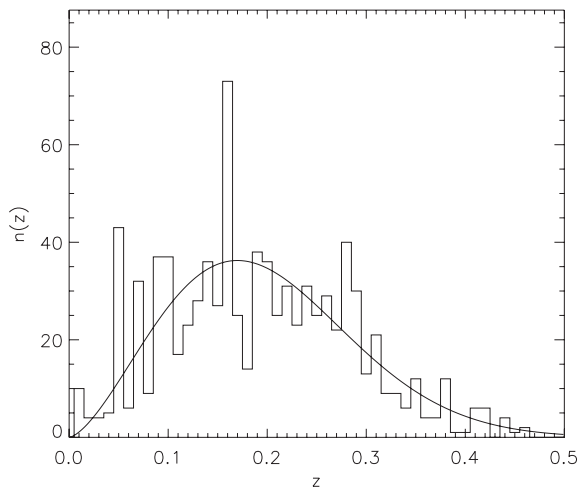
Figure 2. Redshift distribution of our sample of 250-µm sources above 33 mJy, with the reliability, redshift quality and Petrosian *r*-band cuts applied (see the main text for details). The smooth solid line is a fit to the distribution of all selected redshifts: $n(z) = z^{1.5}e^{7.0-26z^2}$.

solutions), we fit the redshift distribution to a function of the form $n(z) = z^{1.5}e^{a-bz^2}$. The best fit to our observed distribution is for $a = 7.0$ and $b = 26$ (shown as a smooth solid line in Fig. 2).

3 METHODS

3.1 Estimating the angular correlation function

The standard estimator for measuring angular correlations is $w_{LS} = (DD - 2DR + RR)/RR$ (Landy & Szalay 1993), where DD, DR and RR are the (normalized) galaxy–galaxy, galaxy–random and random–random pair counts at separation θ. We employ a more abundant random catalogue (by a factor of 10) that Poisson samples the same survey region as our observed catalogue. The normalization takes out the overabundance of the random catalogue by scaling the DR and RR counts accordingly. For the estimate of $w(\theta)$ and its errors we use the Jackknife technique (e.g. Wall & Jenkins 2003, Norberg et al. 2009), employing 4×4 regions and estimating errors from the Jackknife sampling variance.

The estimator is to be fitted by its expected value $1 + \langle w_{LS} \rangle = [1 + w(\theta)]/(1 + w_\Omega)$, where the 'integral constraint' w_Ω is the integral of the model for the two-point correlation function over the survey area. We consider a two-parameter fit for the generic power law $w(\theta) = (\theta/A)^{-\delta}$, as well as a single parameter fit for A with constant slope $\delta = 0.8$. Van Kampen et al. (2005) give details on the fitting technique, which employs non-linear χ^2-fitting using the Levenberg–Marquardt method (Press et al. 1988). This allows us to easily take into account the integral constraint, but also produces the covariance matrix of the fitted parameters which provides a good estimate of their uncertainties.

For small samples, the estimates depend somewhat on the way the data are binned. For this reason we have used a range of bin sizes and intervals over which we bin the angular separations, and adopt the one that produces the smallest fractional uncertainties in the jackknife estimates. Furthermore, there is some evidence of a feature in the angular correlation function near the filter scale of 2 arcmin used in the source detection, so we excluded the corresponding bin from the fit. This was only found to be important for the full sample (as demonstrated by the fourth data point in Fig. 3): no difference was seen for the subsamples introduced in Section 4.2.
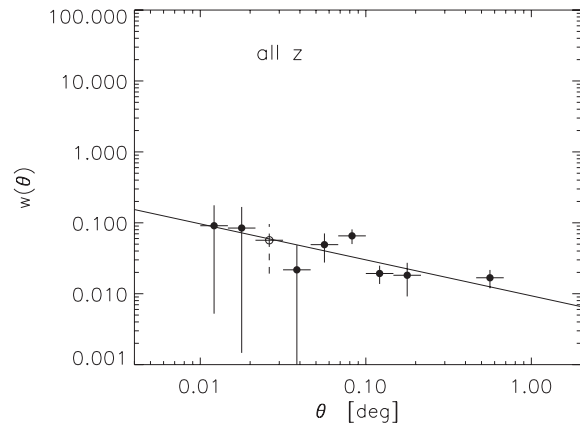

Figure 3. Angular correlation functions for all 250-µm galaxies in the SDP field (i.e. the sample shown in the top panel of Fig. 1). The solid line shows the two-parameter fit, where the fitted parameter values can be found in the top row of Table 1. The open symbols represent negative values for the estimated correlation function. Errors are obtained using the Jackknife technique (see the main text for details).

3.2 Spatial correlation length from $w(\theta)$

The traditional method (e.g. Peebles 1980) for estimating the spatial clustering length r_0 is to measure the angular correlation function and the redshift distribution, and then use Limber's equation (Limber 1953) to derive r_0. We employ the code used by Farrah et al. (2006), assuming a smooth redshift distribution of the form $n(z) = z^{1.5}e^{a-bz^2}$ that is fitted to the observed redshift distribution.

Because our analysis is limited to low redshift ($z < 0.3$), the precise choice for the assumed evolution of the correlation function does not matter too much: assuming 'stable clustering' (fixed in physical coordinates) of 'comoving clustering' (fixed in comoving coordinates) does not change the results much for $z < 0.3$ (most terms scale with $1 + z$), especially because we primarily consider redshift slices of thickness $\Delta z = 0.05$.

4 RESULTS

4.1 Angular clustering without redshift information

We first look at the angular correlation function of all submm galaxies detected by SPIRE at the 5σ level, i.e. the sample shown in the top panel of Fig. 1. Most of these galaxies do not have measured redshifts, but because of the strong negative *K*-correction at these wavebands we expect a wide range of redshifts (see also Amblard et al. 2010).

The resulting angular correlation function, along with a two-parameter power-law fit, is shown in Fig. 3, and displays very little clustering, as was already shown by Maddox et al. (2010) for the slightly larger full SDP data set (that is, including the small region that is not part of the GAMA area). This should just be seen as a confirmation of the earlier results, and is included here to demonstrate consistency.

4.2 Angular clustering in redshift slices

As redshift information is only reasonably complete for $z < 0.3$, we now restrict ourselves to these low redshifts. We first consider the whole range $0 < z < 0.3$, which is the sample for which the

spatial distribution on the sky is shown in the bottom panel of Fig. 1. The SDP field is rotated by 25°, so our *x* and *y* coordinates represent a rotated coordinate system with respect to the usual RA and Dec. axes.

The angular clustering estimate for these 724 sources is shown in the top-left panel of Fig. 4(a), along with the two-parameter fit to this estimate. We see that the $z < 0.3$ angular clustering signal is fairly low for the two-parameter fit, with a large uncertainty on the clustering amplitude (see Table 1); the dilution of any intrinsic clustering signal due to the long line of sight (of order 30 times the width of the lightcone) is apparently too severe. If we fix the slope at $\delta = 0.8$ (as shown in Fig. 4b), we find a more significant

one-parameter fit for the amplitude, although the uncertainty is still considerable.

To remove some of the dilution of the clustering signal due to projection along the line of sight, we cut the lightcone in redshift slices. Given the measured redshift distribution, as shown in Fig. 2, we selected redshift slices such that these are as thin as possible but still contain a sufficient number of sources for a reliable clustering estimate. We start at $z = 0.05$, where the redshift distribution starts to pick up, and end at $z = 0.3$, as the redshift distribution drops sharply there. Our clustering estimator works well for over a hundred sources, which allows for a redshift interval of $\Delta z = 0.05$ for the present sample (for the full *Herschel*-ATLAS data set we
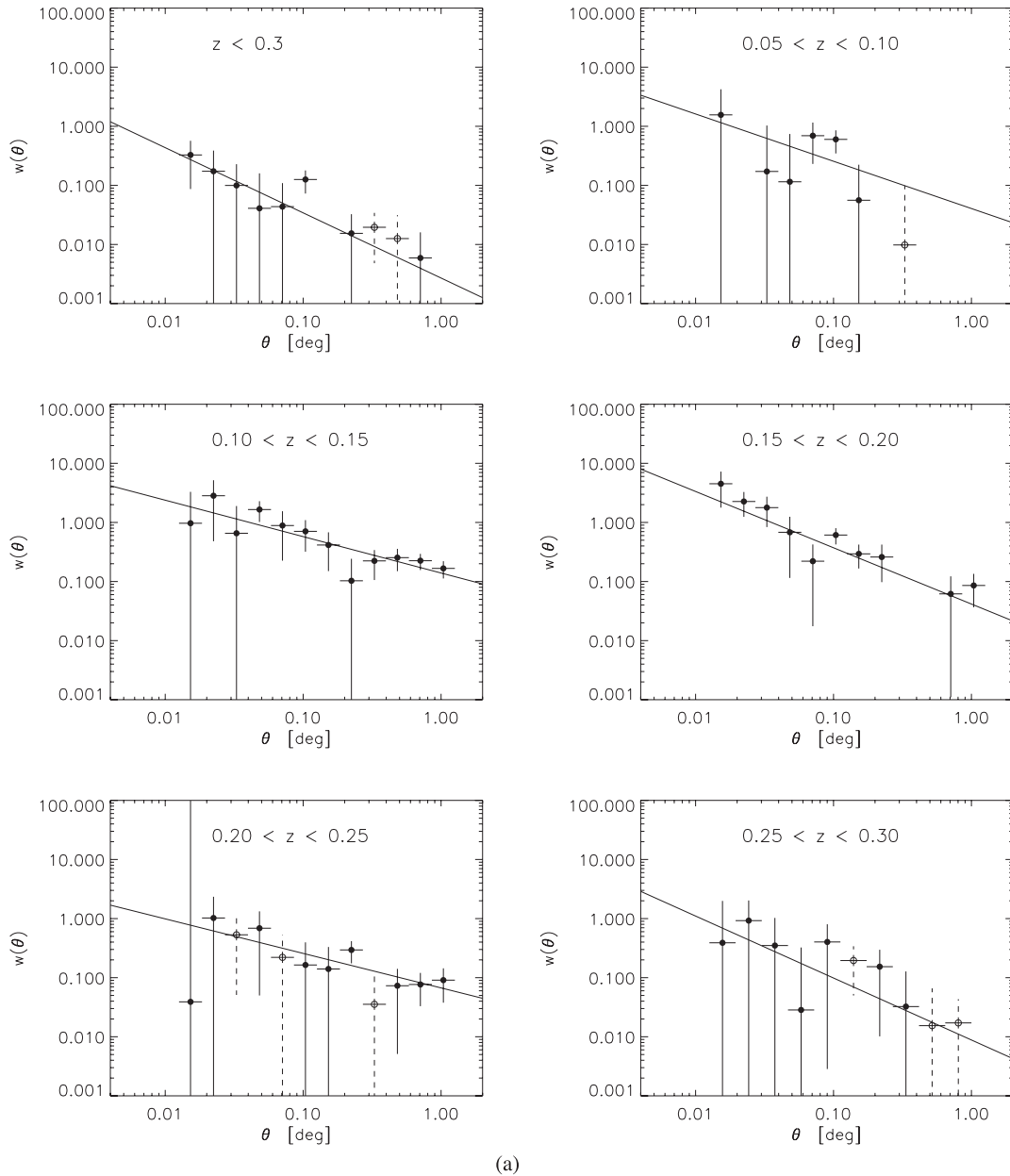

(a)

Figure 4. (a) Angular correlation functions for $0 < z < 0.3$ (top-left panel) and for each redshift slice, with two-parameter fits shown. The values of the fitted parameters are listed in Table 1. The open symbols represent negative values for the estimated correlation function. Errors are obtained using the Jackknife technique (see the main text for details). (b) Angular correlation functions for $0 < z < 0.3$ (top-left panel) and for each redshift slice, with one-parameter fits shown. The values of the fitted parameters are listed in Table 2. The open symbols represent negative values for the estimated correlation function. Errors are obtained using the Jackknife technique (see main text for details). Please note that the data points are not the same as in Fig. 4(a), as the integral constraint is a function of the fitting parameters but also used to correct the data points (see the main text for details).
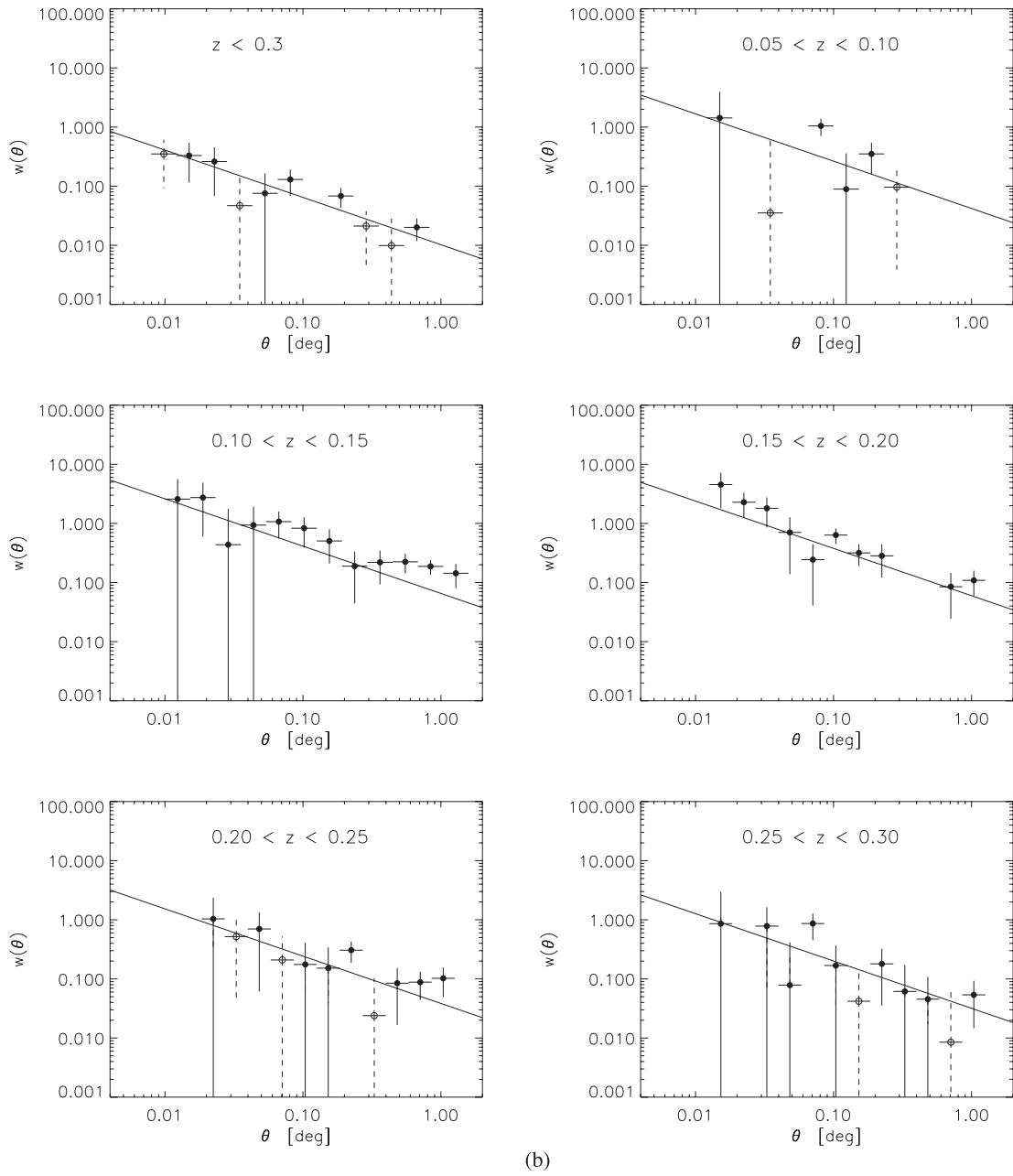
(b)

Figure 4 – *continued*

Table 1. Clustering measures for all samples considered (see the main text for details) for the two-parameter fits. An estimate for r_0 for the 'all z' sample has not been given as its redshift distribution is unknown.

Slice	N	Minimum incompleteness	A (arcmin)	δ	r_0 (Mpc)
all z	5363	–	0.006 ± 0.008	0.51 ± 0.09	–
$z < 0.3$	724	14 per cent	0.28 ± 0.33	1.10 ± 0.39	6.34 ± 5.44
$0.05 < z < 0.10$	123	1.1 per cent	1.09 ± 0.97	0.80 ± 0.29	3.23 ± 2.19
$0.10 < z < 0.15$	137	2.3 per cent	2.45 ± 1.20	0.62 ± 0.15	4.47 ± 1.72
$0.15 < z < 0.20$	167	7 per cent	2.13 ± 0.62	0.95 ± 0.19	7.20 ± 1.81
$0.20 < z < 0.25$	136	20 per cent	0.59 ± 0.66	0.58 ± 0.19	3.02 ± 2.50
$0.25 < z < 0.30$	145	39 per cent	0.66 ± 0.86	1.05 ± 0.83	5.13 ± 5.50

Table 2. Clustering measures for all samples considered (see the main text for details) for the one-parameter fits (fixed slope: $\delta = 0.8$). An estimate for r_0 for the 'all z' sample has not been given as its redshift distribution is unknown.

Slice	N	$A_{0.8}$ (arcmin)	r_0 (Mpc)
all z	5363	0.04 ± 0.02	–
$z < 0.3$	724	0.20 ± 0.04	5.62 ± 1.14
$0.05 < z < 0.10$	123	1.14 ± 0.38	3.29 ± 1.10
$0.10 < z < 0.15$	137	1.99 ± 0.51	5.23 ± 1.33
$0.15 < z < 0.20$	167	1.78 ± 0.31	5.68 ± 1.00
$0.20 < z < 0.25$	136	1.20 ± 0.30	5.21 ± 1.31
$0.25 < z < 0.30$	145	1.13 ± 0.26	5.42 ± 1.26

should be able to adopt thinner slices). This gives us five redshift slices in all.

The resulting angular clustering estimates are shown in Fig. 4(a) for the two-parameter fits, and in Fig. 4(b) for the one-parameter fits. Note that the integral constraint (see Section 3.1) is a function of amplitude A and slope δ, but is also used to correct the data points. This results in somewhat different data points in Figs 4(a) and (b) (best seen at the larger angles), as the fitted values for A and δ for the two-parameter fit will be different from the fitted value for A and the choice $\delta = 0.8$ for the one-parameter fit.

The fitting parameters corresponding to the estimates shown in Figs 4(a) and (b) are listed in Tables 1 and 2, for the two- and one-parameter fits, respectively, where N is the number of sources in each slice. The spatial clustering length r_0, as listed in the last column of each table, is discussed in the following section.

For the one-parameter fit a fixed slope with $\delta = 0.8$ was adopted, as found for local, optically selected galaxies. This value is also consistent with all fitted slopes found from the two-parameter fit, taking the uncertainties into account. It might therefore be argued that adopting a fixed slope $\delta = 0.8$ is a good approximation and helps to produce a tighter constraint on the clustering amplitude. Still, for both the two- and one-parameter models we obtain a good fit for each of the redshift slices, even though the angular correlation function measure itself can be noisy for some of the redshift slices. The best determinations are for the bins around the peak of the redshift distribution, where we find the most significant values for the fitting parameters. The slope is in all cases consistent with that for normal galaxies, i.e. around $\delta \approx 0.8$, even though uncertainties can be considerable, and certainly for the higher redshift bins is somewhat self-induced due to the optical selection (see Section 2.2) and the choice $\delta = 0.8$ for the fixed slope in the case of the one-parameter fits. This is discussed further in Section 5.

4.3 Spatial clustering

In order to use the Limber equation inversion to estimate the spatial clustering strength we need to use the redshift distribution, as shown in Fig. 2. Because of the relatively small field of view, this distribution shows quite a bit of variance. To ensure that the necessary numerical integrations are well behaved, we fit a continuous function of the form $z^{1.5} e^{a-bz^2}$ to the observed redshift distribution, which is shown in Fig. 2 as a smooth solid line. For the fitting parameters we found $a = 7.0$ and $b = 26$. The redshift distribution for all sources is unknown at this point, so we do not estimate a spatial clustering length for the full sample (first row in Table 1).

We then compute the spatial correlation length r_0 for each redshift slice using the Limber equation inversion technique (see Sec-

tion 3.2), for both the two- and one-parameter fits, assuming comoving clustering (if we assume stable clustering we obtain values for r_0 which are roughly 10 per cent larger). For the spectroscopic redshifts we need not worry much about the redshift errors, as these are much smaller than the thickness of the slices (i.e. $\Delta z = 0.05$).

The resulting values for r_0 are listed in Tables 1 and 2, respectively, in units of Mpc. As the resulting value is sensitive to the slope of the angular correlation function, we obtain different results for the two- and one-parameter fits when the fitted slope (for the two-parameter fit) is different from 0.8. Because of the significant uncertainties in the estimates of the clustering lengths, it is premature to study the evolution of clustering with this data set. What is interesting is that the slices are sufficiently thin to clearly detect clustering, which is not the case for the larger redshift range $0 < z < 0.3$. Once the whole area of *Herschel*-ATLAS is covered, we should be able to reduce uncertainties to such a level where we can systematically study clustering trends with redshift.

4.4 A structure at $z = 0.164$

The redshift distribution of our selected source population, as shown in Fig. 2, displays a fairly pronounced peak near $z \approx 0.16$. If we zoom in on the redshift distribution around this peak, as plotted in Fig. 5 (top panel), we see that the peak is split into two, with the largest part centred around $z = 0.164$. Plotting the distribution of the corresponding sources (Fig. 5, bottom panel) around this redshift, in the interval $0.162 < z < 0.166$, we see a clear structure appearing. The thickness of this redshift slice is around 15 Mpc, whereas at this redshift the field of view is around 34 Mpc, so we are likely seeing filamentary structure mostly aligned with the plane of the sky.

Maddox et al. (2010), who performed the first angular clustering analysis of this field, pointed out that there are patchy wisps of cirrus that plague the SDP field. However, this does not seem to align with the 'filamentary structure' shown in Fig. 5. Comparing to the distribution of galaxies selected in the optical, that is, all GAMA galaxies with redshifts $0.162 < z < 0.166$ and $r_{\rm Pet} < 19.4$ (bottom panel of Fig. 5), we see a similar filamentary structure, tracing the low-redshift submm galaxy distribution fairly well, but also displaying several distinct galaxy groups which are absent in the low-redshift submm galaxy distribution. In Fig. 6 we plot this same population of GAMA galaxies along the line of sight, which clearly shows the overdensity of galaxies at $z = 0.164$ to be produced by several groups and filaments roughly perpendicular to the line of sight. The $z = 0.164$ structure might be responsible for the somewhat larger clustering length seen in the $0.15 < z < 0.2$ redshift bin (see Fig. 4 and Tables 1 and 2), although the excess is marginally significant.

5 CONCLUSIONS

We selected a sample of 250-μm sources, detected at the 5σ level, from the *Herschel*-ATLAS SDP data, and used the cross-match with the GAMA catalogue to assign redshifts to as many of these sources as possible, taking care to only use reliable IDs and spectroscopic redshifts of sufficient quality, and exploiting the near completeness of the GAMA spectroscopic redshifts for $r_{\rm Pet} < 19.4$. Because the redshift distribution drops off fairly quickly beyond $z \approx 0.3$, we restricted our analysis to $z < 0.3$.

Simply taking all 250-μm sources and ignoring any redshift information reproduces the result of Maddox et al. (2010) for the same data set: no clear clustering signal for these ∼5000 sources.
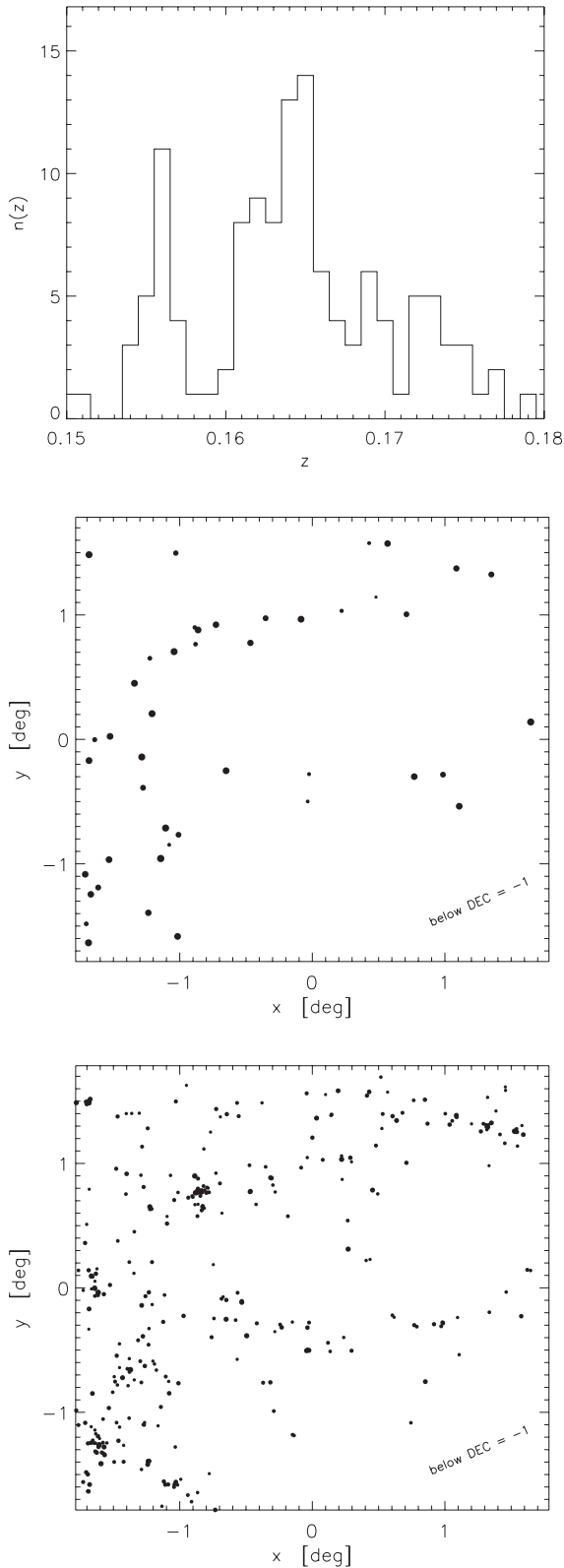
Figure 5. A structure at $z = 0.164$. The top panel shows a zoom-in on the redshift distribution around the spike that is prominently visible in Fig. 2. submm sources in the redshift slice $0.162 < z < 0.166$, with all other selection criteria applied (see Section 2.2), are shown in the middle panel. For clarity, symbol sizes are three times larger than for Fig. 1. The bottom panel displays all $r_{Pet} < 19.4$ GAMA galaxies with redshifts in the same $0.162 < z < 0.166$ slice.
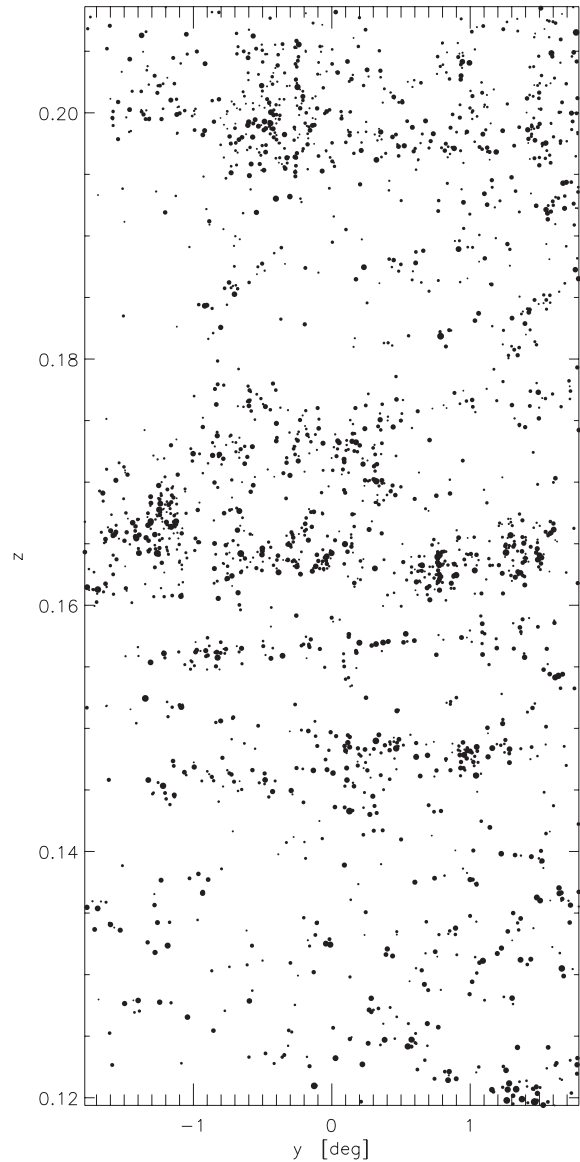

Figure 6. The $z = 0.164$ structure along the line of sight seen in GAMA for all galaxies with redshifts and $r_{Pet} < 19.4$. The 'y' coordinate is the same as used in Figs 1 and 5, i.e. one of the coordinates of the SDP field that is rotated by $25°$ with respect to RA and Dec.

Taking just the 910 galaxies at $z < 0.3$ that satisfy our selection criteria, we do detect clustering. When we subdivide these galaxies into redshift slices of thickness $\Delta z = 0.05$ we detect a significant clustering signal for most of the slices. Clearly the dilution of the clustering signal along the line of sight is too strong for the relatively small area we have covered for the SDP data, but the results for the slices show that for the full area of *Herschel*-ATLAS we should be able to cleanly detect a clustering signal, and study how this evolves with redshift.

In a related paper, Guo et al. (2011) measured the cross-correlation function of the *Herschel*-ATLAS SDP and GAMA sources, but also their autocorrelation functions. They used a different method, but for a similar sample. Their estimate for the spatial clustering length of 4.76 ± 0.63 Mpc, obtained for a redshift distribution peaking at $z = 0.19$, is consistent with our measures for the (thinner) redshift slices in the same range (both for the two- and one-parameter fits). Even though our clustering lengths are somewhat

larger in most of our bins, the uncertainties are too large to establish whether there is a significant discrepancy between our results: we will need the full area of *Herschel*-ATLAS to test this.

Our estimates for the five redshift slices (in the range $0.05 < z < 0.3$) give a mean spatial clustering length of 4.6 ± 3.4 Mpc for the two-parameter fits, and 5.0 ± 1.2 Mpc for the one-parameter fits (the smaller error is due to the assumption for the slope of the correlation function). These values are very close to what is found for optically selected galaxies in the SDSS: Zehavi et al. (2011) found spatial clustering lengths between roughly 4 and 10 Mpc, depending on the absolute luminosity threshold adopted, with r_0 increasing for increasingly brighter thresholds. Most of their subsamples have r_0 in the range 5–6 Mpc. For our special selection criteria we have a distribution over optical luminosities that is not sharply cut-off, so a straightforward comparison cannot be made, although our spatial clustering lengths are in the same range. From this point of view, our $z < 0.3$ 250-µm selected galaxies do not appear to be very different from optically selected galaxies, edging towards blue galaxies (e.g. Coil et al. 2008; Zehavi et al. 2011; Christodoulou et al. 2012), which would indicate that our sample consists mostly of moderately star-forming galaxies. We will investigate this in more detail for the full *Herschel*-ATLAS sample.

One caveat in the comparison to optically selected galaxies is that our samples are not complete in the submm band due to the optical limit $r_{Pet} < 19.4$, which means that we miss low-redshift galaxies with $r_{Pet} > 19.4$ that are still bright enough in the submm to be included in our sample. In Section 2.2 we introduced and estimated the minimum fraction missed for each of our subsamples (listed in Table 1). This is a minimum fraction as the photometric redshifts used in this estimate go deeper (to $r_{Pet} \sim 20.8$) but still do not include all possible $z < 0.3$ submm galaxies. For the lowest redshift slices this fraction is small, so the conclusion that submm galaxies in that redshift range cluster like optical galaxies is fairly robust. However, for the highest redshift slice ($0.25 < z < 0.3$) the incompleteness is at least 39 per cent, and the optical selection starts to become fairly dominant, making the comparison to a fully optically selected sample somewhat self-induced.

A more general caveat is that any incompleteness in the sample could bias the clustering estimate if any of our (sub)samples is not fair, i.e. not a good representation of the submm (sub)sample that would include all $r_{Pet} > 19.4$ sources as well. As the incompleteness at low redshifts is minor, for the lowest redshift slices this is not a worry, but for the higher redshift slices the samples are relatively incomplete and might be biased. This will have to be investigated further using the Phase 1 data set, where we will also use other methods to estimate the spatial clustering length.

Finally, we found an interesting structure in the redshift cone, at $z = 0.164$, which is a likely filamentary structure roughly aligned with the plane of the sky. It is also seen to have several galaxy groups in the optical waveband which are absent in the sample we selected for the clustering analysis. The sources in these groups will provide excellent targets for follow-up studies with instruments such as ALMA that have much higher spatial resolution than SPIRE.

ACKNOWLEDGMENTS

REFERENCES

Abazajian K. N. et al., 2009, ApJS, 182, 543
Almaini O. et al., 2003, MNRAS, 338, 308
Amblard A. et al., 2010, A&A, 518, L9
Baldry I. K. et al., 2010, MNRAS, 404, 86
Blain A. W., Chapman S. C., Smail I., Ivison R., 2004, ApJ, 611, 725
Christodoulou L. et al., 2012, MNRAS, 425, 1527
Coil A. L. et al., 2008, ApJ, 672, 153
Cooray A. et al., 2010, A&A, 518, 22
Driver S. P. et al., 2009, Astron. Geophys., 50, 5.12
Driver S. P. et al., 2011, MNRAS, 413, 971
Eales S. et al., 2010, PASP, 122, 499
Farrah D. et al., 2006, ApJ, 641, L17
Griffin M. et al., 2010, A&A, 518, L3
Guo Q. et al., 2011, MNRAS, 412, 2277
Hill D. T. et al., 2011, MNRAS, 412, 765
Landy S. D., Szalay A. S., 1993, ApJ, 412, 64
Limber D. N., 1953, ApJ, 117, 134
Maddox S. J. et al., 2010, A&A, 518, L11
Nguyen H. T. et al., 2010, A&A, 518, L5
Norberg P., Baugh C. M., Gaztañaga E., Croton D. J., 2009, MNRAS, 396, 19
Pascale E. et al., 2011, MNRAS, 415, 911
Pearson E. A. et al., 2012, MNRAS, submitted
Peebles P. J. E., 1980, The Large-Scale Structure of the Universe. Princeton Univ. Press, Princeton, NJ
Pilbratt G. L. et al., 2010, A&A, 518, L1
Press W. H., Flannery B. P., Teukolsky S. A., Vetterling W. T., 1988, Numerical Recipes: The Art of Scientific Computing. Cambridge Univ. Press, Cambridge
Rigby E. E. et al., 2011, MNRAS, 415, 2336
Robotham A. S. G. et al., 2010, PASA, 27, 76
Scott S. E., Dunlop J. S., Serjeant S., 2006, MNRAS, 370, 1057
Short J., Coles P., 2011, MNRAS, 412, L93
Smith D. J. B. et al., 2011, MNRAS, 416, 857
Sutherland W., Saunders W., 1992, MNRAS, 259, 413
van Kampen E. et al., 2005, MNRAS, 359, 469
Wall J. V., Jenkins C. R., 2003, Practical Statistics for Astronomers. Cambridge Univ. Press, Cambridge
Webb T. M. et al., 2003, ApJ, 587, 41
Weiß A. et al., 2009, ApJ, 707, 1201
Zehavi I. et al., 2011, ApJ, 736, 59

This paper has been typeset from a TEX/LATEX file prepared by the author.